Enhancement of magnetic properties in compressively strained $PrVO_3$ thin films

D. Kumar,[1] A. Fouchet,[1] A. David,[1] A. Cheikh,[1] T. S. Suraj,[2] O. Copie,[3] C. U. Jung,[4] A. Pautrat,[1] M. S. Ramachandra Rao,[2] and W. Prellier[1,*]

[1]*Laboratoire CRISMAT, CNRS UMR 6508, ENSICAEN, Normandie Université, 6 Bd Maréchal Juin, F-14050 Caen Cedex 4, France*

[2]*Department of Physics, Nano Functional Materials Technology Centre and Materials Science Research Centre, Indian Institute of Technology Madras, Chennai 600036, India*

[3]*Institut Jean Lamour, UMR 7198, CNRS/Université de Lorraine, 54011 Nancy, France*

[4]*Department of Physics, oxide research center, Hankuk University of Foreign Studies, Yongin, Gyeonggi 17035, Korea*

(Received 4 April 2019; published 24 December 2019)

Strain engineering is an important issue in oxide thin films to explore new functionalities. Here a series of high quality epitaxial $PrVO_3$ (PVO) thin films were grown, by pulsed laser deposition (PLD) technique, as a function of thickness on (La,Sr)(Al,Ta)O_3 (100) [LSAT (100)] and $LaAlO_3$ (100) [LAO (100)] substrates with a nominal lattice mismatch of -0.8% and -2.9%, respectively. X-ray diffraction revealed a constant *out-of-plane* lattice parameter of PVO/LSAT with an increase in film thickness, and a rather continuous decrease for PVO/LAO films. Whereas thicker PVO films show a ferromagneticlike behavior, at low thickness a surprising decrease of coercivity (H_c) and increase of saturation magnetization (M_s) is observed. This behavior is described by using a model of a "dead layer" which possesses a strong paramagnetic susceptibility. Our XPS investigations further reveal the formation of V^{4+} at the surface of the film to be responsible for this paramagnetic dead layer, which is reduced by adding a capping layer on top of the PVO film. Finally, the Néel temperature (T_N) is examined as a function of film thickness, and found to vary between 25 and 30 K for LSAT and LAO, respectively. These results pave the way for the use of vanadate in thin film devices.

DOI: 10.1103/PhysRevMaterials.3.124413

I. INTRODUCTION

The perovskite oxides with generic formula ABO_3 have attracted a great deal of scientific interests thanks to the strong correlation between orbital (electronic), spin (magnetic), and lattice degrees of freedom (structural). Owing to various functional properties such as ferroelectricity, ferromagnetism, antiferromagnetism, colossal magnetoresistance, and superconductivity, the oxides are thus exploited in the diverse technological applications for electronics, data storage or sensing, and so on [1–4]. While for bulk materials these underlying properties can be expanded via lattice distortion by applying hydrostatic pressure [5,6], a substrate-induced biaxial strain in ABO_3 epitaxial thin films has also been proved to be an effective tool to modify the spin-orbit-lattice coupling [7–10]. Among RVO_3 (R: rare earth element), the bulk $PrVO_3$ (PVO), at room temperature, adopts an orthorhombic *Pbnm* crystal structure with the lattice parameters: $a_o = 5.487$ Å, $b_o = 5.564$ Å, and $c_o = 7.778$ Å (o stands for orthorhombic) [11]. In the following we will consider the pseudocubic unit cell of PVO that yields $a_{pc} \approx a_o/\sqrt{2} \approx b_o/\sqrt{2} \approx c_o/2 \approx 3.901$ Å (pc stands for pseudocubic). The bulk PVO is an antiferromagnet associated with C-type spin ordering (C-SO), where V spins are staggered in the ab plane and aligned ferromagnetically along the c axis, with $T_N \simeq 130$ K [12]. However, for a PVO thin film, the DFT calculations reveal a G-type spin ordering (G-SO) in the ground state (where V spins are aligned antiferromagnetically along all three crystal directions), associated with a C-type orbital ordering (C-OO) through the Kugel-Khomskii mechanism [13,14]. In the course of our previous study, we revealed a pathway to tune the magnetic properties of PVO thin films grown on $SrTiO_3$ (STO) substrate by monitoring the concentration of oxygen vacancies in PVO films [13]. A careful crystal structural investigation revealed that the tensile-strained PVO film on STO substrate adopts a monoclinic $P2_1/m$ crystal lattice [10,13,15]. In addition, we have scrutinized the effect of substrate-induced strain upon the structural and magnetic properties by growing PVO films on top of various lattice mismatched perovskite-oxide substrates [10]. The study revealed that a large compressive strain in PVO films not only promotes the superexchange interaction, i.e., V-V interactions, but also changes the electronic structure of PVO. Recent investigations have unveiled that the layer-by-layer control of film through minute deposition tunes the strain states in a film, offering fascinating functional properties, namely spin-glass behavior in compressively strained $BiFeO_3$ thin films [16], thickness-dependent magnetic anisotropy in $La_{2/3}Ca_{1/3}MnO_3$ films [17], and the dimensional crossover of magnetization from 3D to 2D in $SrRuO_3$ thin films with a decrease in film thickness [18]. Even if the RVO_3 system is a good candidate to exhibit the spin-orbit-lattice coupling, only a few film thickness-dependence studies have however been conducted in thin films [19,20].

In this paper we study the thickness-dependent structural and magnetic properties of the $PrVO_3$ (PVO) thin films grown on (La,Sr)(Al,Ta)O_3 (LSAT) and $LaAlO_3$ (LAO) substrates. While thick PVO films (100 nm) remain strained to the LSAT

*wilfrid.prellier@ensicaen.fr

 ©2019 American Physical Society

substrates, films of ∼50 nm show partial relaxation on the LAO substrates. We evidence a dead layer at the film surface which possesses strong paramagnetic susceptibility, and is at the origin of observed magnetic properties. In addition, we explore the possibility to heal this layer by capping witha few layers of LAO, in order to recover the magnetic properties of PVO.

II. EXPERIMENT

The PVO thin films were epitaxially grown on top of (100)-oriented LAO and LSAT substrates, within a thickness range of 10 to 100 nm, by using the pulsed laser deposition (PLD) technique. A KrF excimer laser ($\lambda = 248$ nm) with a repetition rate of 2 Hz and laser fluence of 2 J/cm^2 was focused on a $PrVO_4$ ceramic target, with a substrate-to-target distance of 5 cm. The films were deposited at a growth temperature $T_G = 650\,^{\circ}$C and oxygen partial pressure $P_{O_2} = 10^{-6}$ mbar. To ensure homogeneous oxygen vacancies throughout the growth, the samples were cooled down to room temperature in the same oxygen pressure. The crystallinity and the structure of the PVO films were characterized using x-ray diffraction technique (Bruker D8 Discover diffractometer, Cu $K\alpha 1$ radiation, $\lambda = 1.5406$ Å). The surface morphology of the films was investigated using atomic force microscopy (AFM) PicoSPM. The magnetic measurements were performed using a superconducting quantum interference device (SQUID) magnetometer as a function of magnetic field H (parallel configuration) and temperature T. The magnetization-magnetic field (M-H) hysteresis curves were obtained at $T = 20$ K and magnetization-temperature (M-T) data were carried out at $H_{\text{in-plane}} = 50$ Oe. The x-ray photoemission spectroscopy (XPS) was performed by using Al k_α excitation ($h\nu = 1486.6$ eV) x-ray source, operated at 10 mA and 10 kV. The base pressure of the analyzer chamber was maintained around 5×10^{-7} mbar and operated in a larger area mode by using a hemispherical energy analyzer. The samples were etched by Ar ion sputtering *in situ* in the XPS analysis chamber. The binding energies of all compositions were calculated by employing Shirley background type with reference to the C 1s peak at 284.5 eV. The lattice constants of PVO, LSAT, and LAO in the *pseudocubic* structure are 3.901, 3.868, and 3.791 Å, respectively, establishing PVO to be grown under nominal compressive strain with a lattice mismatch of −0.8% (LSAT) and −2.9% (LAO).

III. RESULTS AND DISCUSSION

Figures 1(a) and 1(b) display θ-2θ x-ray diffraction measurements of a series of PVO films grown on top of (100)-oriented LAO and LSAT substrates, respectively, around $(100)_{\text{pc}}$ (where pc refers to the pseudocubic notation) of each substrate. The clear thickness fringes for PVO/LSAT films confirm uniform thickness, and well-defined film/substrate interface. However, PVO films grown on LAO substrates do not display oscillations, presumably due to the presence of the twin domains in the LAO substrate [21]. The film thickness (t) was calculated using these fringes, the details of which could be found elsewhere [10]. The AFM analysis was performed on each sample, and a surface roughness less than 0.5 nm was observed confirming the high quality of the samples, without the presence of any islands even in the thicker films [Fig. 1(d)]. The *out-of-plane* and *in-plane* lattice parameters were calculated using XRD θ-2θ [Figs. 1(a) and 1(b)] and reciprocal space map scans (Fig. 2), respectively.

Figure 1(c) illustrates the evolution of PVO lattice parameters as a function of the film thickness, for both LAO and LSAT substrates. First, we see that the out-of-plane lattice parameter of all PVO films has increased for both substrates as compared to that of the pseudocubic bulk PVO [solid red line in Fig. 1(c)], which is in perfect agreement with the in-plane compressive strain imposed by the LAO and LSAT substrate. Moreover, the out-of-plane lattice parameter of PVO/LAO decreases continuously (in overall) with an increase of film thickness, although a slight increase between $t = 19.63$ nm and $t = 24.19$ nm, and also between $t = 55.93$ nm and $t = 74.50$ nm is observed, and believed to be because of uncertainty in the calculations of parameters. Second, PVO films grown on the LSAT substrates show a nearly constant out-of-plane lattice parameter with an increase of film thickness, and a slight change is within the experimental accuracy. [The error bars were calculated by fitting the film peak using the Voigt function, and using the relation between the uncertainty in lattice parameter (Δd) and Bragg's angle ($\Delta\theta$): $\Delta d = \frac{\Delta\theta}{\tan\theta}$. d directly derived from the Bragg diffraction expression]. This nearly constant behavior of the out-of-plane lattice parameter of the PVO film on the LSAT substrate can be rather anticipated due to a smaller mismatch between PVO and LSAT substrate (∼−0.8%).

In order to further investigate the thickness-dependent structural evolutions, the asymmetrical reciprocal space maps (RSMs) were recorded for PVO films, around $(103)_{\text{pc}}$ Bragg's peak of LAO and LSAT [see Figs. 2(a) and 2(b) for PVO/LAO and PVO/LSAT, respectively]. We note that the thinner PVO film ($t \leqslant 24$ nm) is in-plane strained when grown onto LAO, whereas thicker films start to relax [Fig. 2(a)], as the position of the films peak along the horizontal Q_{in} axis shifts toward a lower value. This is in perfect agreement with the highly mismatched PVO films grown on the LAO substrate which tend to relax easily over small thickness, due to a decrease in the strain states as the thickness increases. The in-plane lattice parameters of PVO were calculated using these maps (within the instrumental error) (Fig. 2), and the results are plotted as a function of film thickness in Fig. 1(c). On the LAO substrate, the in-plane lattice parameter of the film increases linearly with the film thickness. This behavior is typical of a partially relaxed film, and is in accordance with the decrease of the out-of-plane lattice parameter with an increase in the films thickness, for a film with an ideal Poisson's ratio [22]. On the LSAT substrates, the situation is different as the PVO films are strained with the substrate, even at $t \sim 100$ nm. This is clearly seen in Fig. 2(b) where the horizontal position of the film peak coincides with the one of the LSAT substrate. Thus, the film and substrate have the same in-plane lattice parameter. Also, the film peak width along the q_{in} axis increases slightly with an increase of film thickness, and could be possibly due to the presence of different domains in the PVO film, as shown in the earlier reports [10,13,15]. Moreover, a range of film thickness analyzed by using electron microscopy [10] in combination with pole figures yield the PVO $[001]_o$ axis along

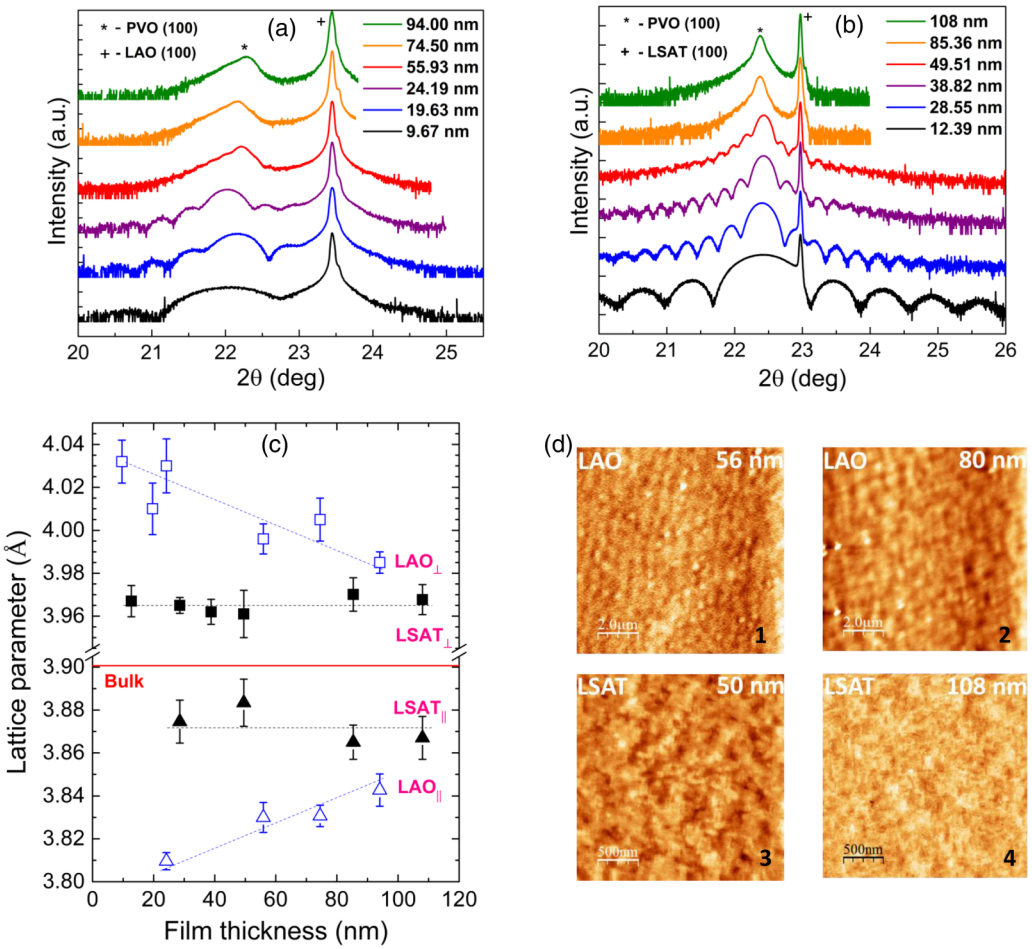

FIG. 1. θ-2θ x-ray diffraction measurements of a series of PVO films grown on (a) LAO and (b) LSAT substrates, around $(100)_{pc}$ of each substrate. The asterisk ($*$) and plus ($+$) represent PVO film and substrate, respectively. (c) Out-of-plane (square symbols in top panel) and in-plane (triangle symbols in bottom panel) lattice parameters of PVO films grown on LAO (blue open symbols) and LSAT (black filled symbols) substrates, as a function of the film thickness, plotted along with the error bars. $\perp$ and $\parallel$ symbols represent the out-of-plane and in-plane lattice parameters of PVO, respectively. The dashed lines serve as a guide to the eyes. The red line indicates a PVO bulk pseudocubic lattice parameter. (d) Typical AFM images of PVO thin films grown on LAO ($10 \times 10\ \mu m^2$) and LSAT ($2.5 \times 2.5\ \mu m^2$) substrates at different thicknesses. The surface roughness (R_q) from 1 to 4 varies as 0.18, 0.43, 0.22, and 0.42 nm, respectively.

an in-plane of film, and thus inducing $[110]_o$-axis growth. A detailed microstructure of the films will be published later. To summarize, the PVO films are strained when grown on the LSAT substrates, even at $t \sim 100$ nm, whereas films of $t \geqslant 50$ nm display partial relaxation when grown on LAO substrates.

Figure 3 details the magnetization-magnetic field (M-H) measurements recorded at $T = 20$ K. In order to clearly observe the PVO magnetic contribution, the diamagnetic backgrounds of the substrates were subtracted from the total measured signal. The magnetic hysteresis cycles for the selected PVO samples are shown in Figs. 3(a) and 3(b) for the LAO substrate and Figs. 3(e) and 3(f) for the LSAT substrate. A clear opening of the hysteresis loop is observed with increasing film thickness, evidencing a low temperature ferromagneticlike behavior of the PVO films. The magnetic moments are however canted, leading to a canted-antiferromagnetic state via antisymmetric spin-spin interaction [$D_{ij}(S_i \times S_j)$, with D_{ij} the Dzyaloshinskii-Moriya term] [15]. Additionally, the magnetization of PVO films could be described as a combination of a soft and a hard magnetic phase, similar to what was observed in orthoferrite $YFeO_3$ [23,24], which is consistent with our previous observations [10]. From Fig. 3 we observe that the thinner films indeed posses a larger soft magnetic phase (paramagnetic) with large saturation magnetization (M_s). In addition, the fraction of film made up of paramagnetic phase reduces, and/or the relative contribution of PVO layer increases simultaneously when film thickness increases. In other words, the contribution of the paramagnetic layer with respect to the total film reduces as film thickness increases. It should also be noted that, with an increase of film thickness, the fraction of the film that represents the paramagnetic phase reduces, but not the amount of paramagnetic material.

The coercive field (H_c) extracted from the hard magnetic phase, saturation magnetization (M_s) and the remanent magnetization (M_R), are plotted as a function of film thickness [Fig. 3(c) for LAO and Fig. 3(g) for LSAT]. A continuous decrease in M_s and increase in H_c are observed for both substrates with an increase in the film's thickness, until a

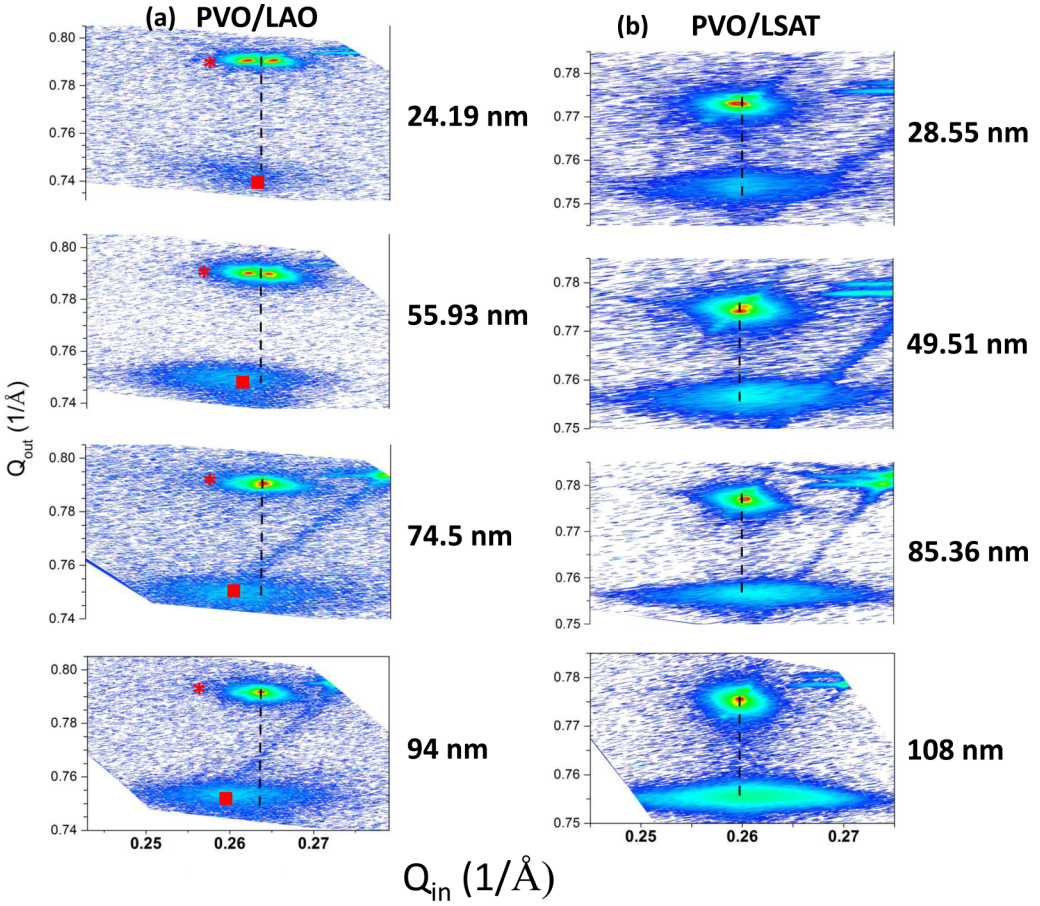

FIG. 2. Asymmetrical reciprocal space maps (RSMs) for a series of PVO thin films grown on (a) LAO and (b) LSAT substrate, recorded around pseudocubic (103) of the substrate. The horizontal axis is Q_{in} and vertical axis is Q_{out} for all RSMs. The substrate and film peaks are located in the upper and lower region of RSMs, and marked by the asterisks and solid square symbols, respectively, for both substrates. The double peak for the LAO substrate is due to twin domains in the substrate. The vertical dashed lines are only a guide to the eyes.

nominal value is reached, which remains nearly constant for the thick films. (This typical trend of M_s and H_c with an increase of film thickness remains true for all measured temperature [25]). Additionally, the shape of the hysteresis loop changes from a squarelike (M-H) to a paramagneticlike S shaped as the thickness is reduced. We suggest here that a large value of M_s for thinner films is reminiscent of the presence of a nonmagnetic/paramagnetic layer at the surface of film, namely a dead layer, similar to the previous observations in $DyTiO_3$ thin films [26]. Actually, when the film surface is exposed to air, the surface of film can get overoxidized, and the magnetic V^{3+} ions can indeed be replaced by V^{4+} or nonmagnetic V^{5+} ions, decoupling Pr^{3+} ions. This overoxidized phase is commonly observed on vanadate films surface such as $LaVO_3$ or $SrVO_3$ [27,28], where the surface of the films is not stable and tends to overoxidize. Such amorphous PVO of a few nanometers on the surface of the film was actually previously observed in the high resolution TEM image of our PVO film on the LAO substrate [10]. This amorphous phase could lead to isolated Pr atoms, which release their strong paramagnetic response. In order to estimate the thickness of the dead layer, we use a model described by Eq. (1) [26], which assumes that this layer is paramagnetic, has null magnetization at remanence, and a huge magnetization at high fields. We then fit the thickness dependence of remanent magnetization (M_R) and saturation magnetization (M_s) with the proposed dead layer model, using the following equation:

$$M_{\text{tot}} = m_{\text{tot}} t = m_P t_P + m_{\text{AF}} t_{\text{AF}}, \tag{1}$$

$$m_{\text{tot}} = (m_P - m_{\text{AF}}) t_P / t + m_{\text{AF}}, \tag{2}$$

where $t = t_P + t_{\text{AF}}$ is the total thickness of the film, t_P is the thickness of the paramagnetic layer, t_{AF} is the thickness of the antiferromagnetic layer, m_P is the moment per unit volume of the paramagnetic layer, and m_{AF} is the moment per unit volume of the antiferromagnetic layer. Setting $m_{\text{AF}} \sim 0.7\ \mu_B$/f.u. (f.u.: formula unit) [29] (for bulk PVO) and $m_P = 0$ (for M_R), a dead layer thickness t_P of ~6 nm for LAO [Fig. 3(d)] and ~4 nm for LSAT [Fig. 3(h)] was obtained by fitting the remanent magnetization. Furthermore, setting m_P to the maximum magnetization of the thinnest sample and using t_P as a fitting parameter, we evaluated $t_P \sim$ 5–6 nm from fitting of M_s vs t (see Ref. [25]).

Remarkably, a similar trend in H_c and M_s was also observed for ferrite thin films, which likely indicates a change in the magnetization spin axis, in addition to a reorientation of the domains above critical thickness [30,31]. In PVO thin films, however, a strong paramagnetic response for thinner

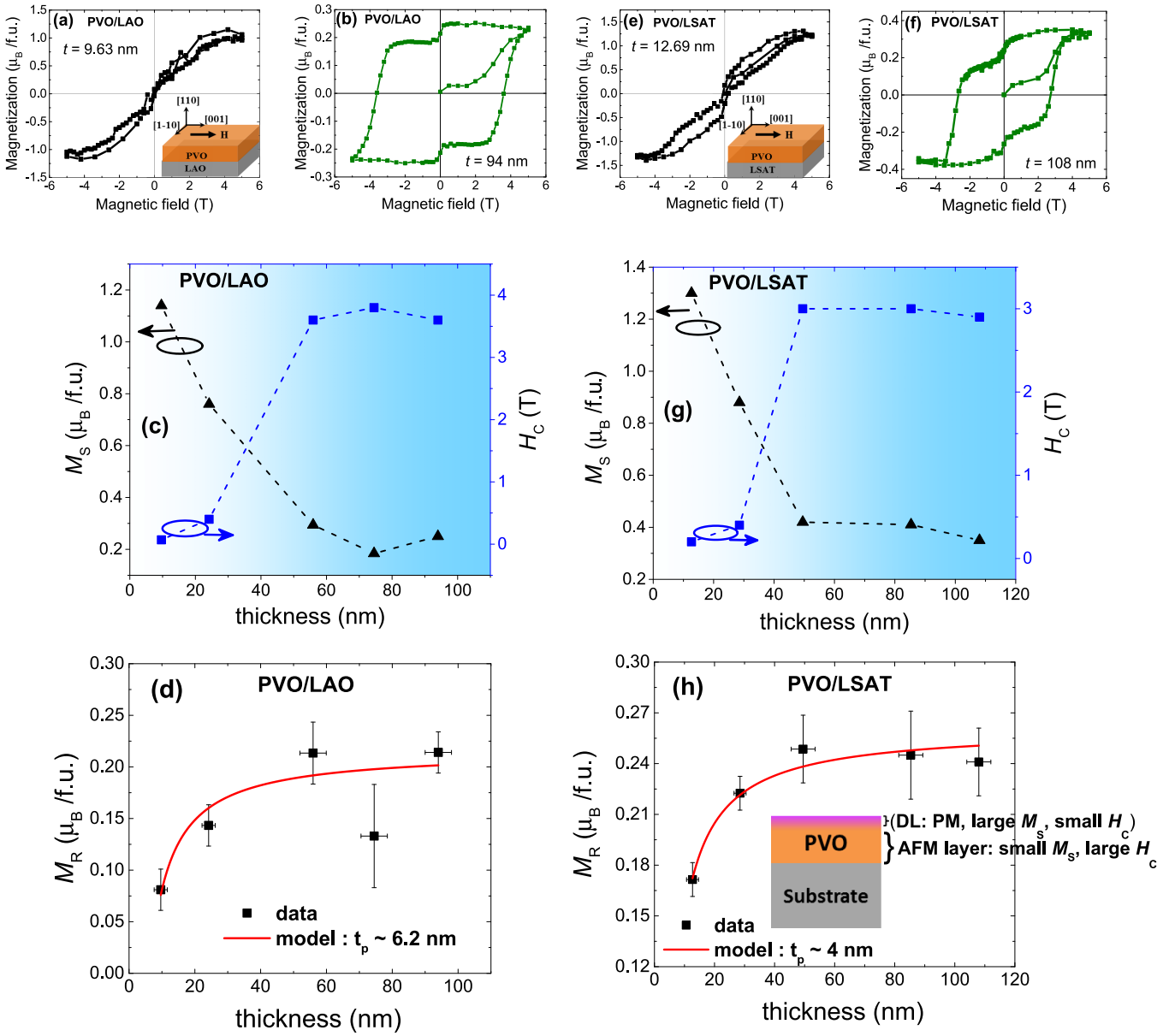

FIG. 3. Magnetization (M) vs in-plane magnetic field (H) measurements obtained at 20 K for: PVO films grown on (001)-oriented LAO substrate, for film thickness (a) $t = 9.63$ nm and (b) $t = 94$ nm, and for PVO/LSAT films (e) $t = 12.69$ nm and (f) $t = 108$ nm. Plot of the saturation magnetization (M_s) (left scale) and magnetic coercivity (H_c) (right scale) as a function of the film thickness for (c) PVO/LAO, and (g) PVO/LSAT films. The shaded area represents thickness range where M_s and H_c almost freeze and does not change with film thickness. Thickness dependence of the remanent magnetization (M_R) for (d) PVO/LAO and (h) PVO/LSAT films. The red line is a fit to M_R vs t plot, using Eq. (2). The right down inset in (a) and (e) represents a schematic of magnetization measurements, where the directions refer to the orthorhombic symmetry of PVO. The inset of (h) is a schematic of a paramagnetic (PM) dead layer (DL) on the surface of the film. The dashed lines are only a guide for the eyes.

films is indicative of a dead layer at the surface of films, which consists of isolated Pr^{3+} atoms. In addition, a decrease of M_s with an increase in film thickness is also evidenced by the decrease in the fraction of the paramagnetic phase, while keeping the thickness of the paramagnetic layer t_P constant. Likewise, the increase of H_c with an increase of film thickness could be related to the increase in the density of pinning sites due to the increase in the number of domains, and/or domain boundaries. Indeed, due to a partial strain relaxation, the film could energetically favor multiple domains, as shown earlier [10]. For thick PVO films, the magnetization and coercive field approach a nominal value, meaning that the magnetic contribution from each layer is static, and independent of film thickness. Nevertheless, the magnetization remains lower than the bulk value (~0.6–0.7 μ_B/f.u.) for thick films, and may be related to the presence of V^{4+}/V^{5+}, which can affect the electron hopping, and thus suppresses the magnetization considerably.

Further magnetic analyses were carried out by performing magnetic measurements as a function of temperature T. For

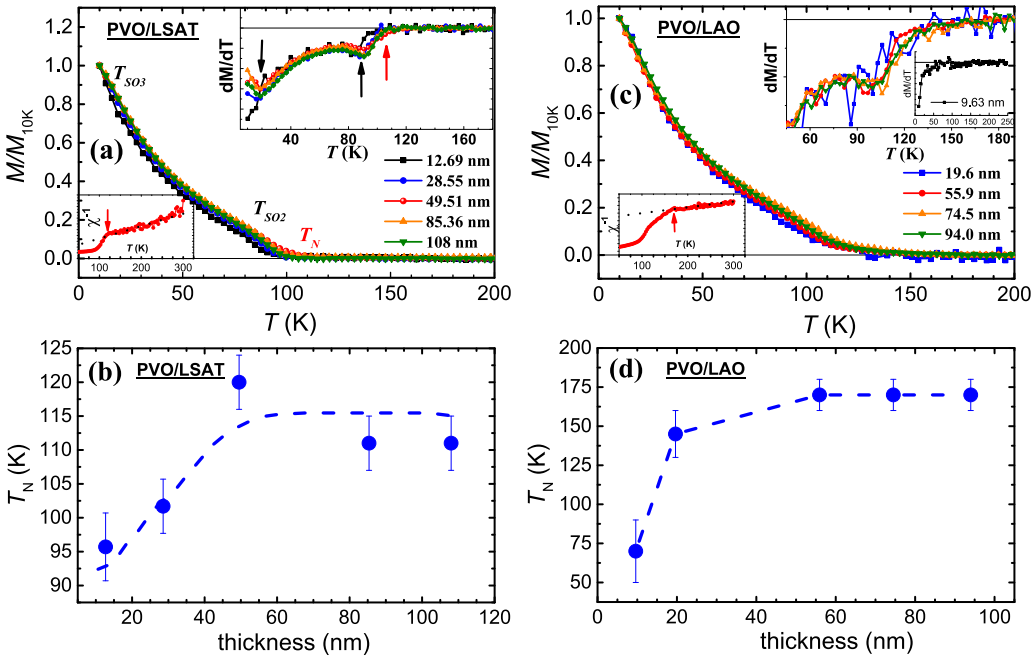

FIG. 4. Normalized magnetization measurements for a series of $PrVO_3$ films grown on top of (a) LSAT and (c) LAO substrate, obtained at $H_{||} = 50$ Oe, displaying different transitions at T_{SO1}, T_{SO2}, and T_{SO3}. The inset is dM/dT for respective substrates. (b) T_N (T_{SO1}) as a function of film thickness for (b) PVO/LSAT and (d) PVO/LAO films. The dashed lines are only a guide to the eyes.

clarity, only field cooled (FC) measurements are shown in Figs. 4(a) and 4(c) for LSAT and LAO substrate, respectively. On the LSAT substrate, PVO films show three distinct anomalies at temperatures T_N, T_{SO2}, and T_{SO3} [Fig. 4(a)] while sweeping the temperature from 300 to 10 K [further confirmed by plotting dM/dT and $\chi^{-1}(T)$]. The rising signal at temperature T_N shows the onset of G-type spin ordered state of the vanadium moments, where these moments align antiferromagnetically ($\|$ to $[001]_o$ axis) along the three crystal axis directions, i.e., in-plane and out-of-plane. While for bulk $PrVO_3$, the transition at T_N was previously ascribed to the onset of a C-type SO of the canted vanadium moments [11,29], for epitaxial $PrVO_3$ thin films, the substrate-induced strain results in a G-type SO, as evidenced by the DFT calculations [13]. The T_N displayed by PVO films on LSAT substrates is clearly shown in the inset of Fig. 4(a), and plotted as a function of film thickness in Fig. 4(b). This depicts the tunability of T_N in the range of 25 K for PVO films grown on LSAT substrates by varying film thickness. Moreover, PVO films exhibit additional magnetic features at temperatures T_{SO2} and T_{SO3}, established by two kinks in MT (in dM/dT as well) at ~90 and 20 K, respectively [Fig. 4(a)]. These orderings are however absent in the bulk PVO, but have been seen in RVO_3 compounds with smaller R size, e.g., $DyVO_3$, $TbVO_3$, and so on [32–34]. The origin of the magnetic feature at T_{SO2} has two alternative explanations. First, it might be due to magnetic polarization of the praseodymium sublattice in the presence of exchange field produced by the vanadium moments, via Pr-V exchange, resulting in a ferrimagnetic structure [34]. Second, it could be due to the reorientation of the vanadium spin configuration from G type to C type, where V^{3+} spins are staggered in the ab plane and aligned ferromagnetically along the c axis. Finally, the transition at T_{SO3} might represent the onset of ferromagnetic (FM) ordering of Pr sublattice, and/or an AFM coupling between Pr^{3+} $4f$ and V^{3+} $3d$ moments. Although the Pr^{3+} moments are canted, giving rise to a finite magnetic moment (~1.1 μ_B), as explained by Reehuis *et al.* for $Pr_{1-x}Ca_xVO_3$ and bulk RVO_3 (R = Ce, Dy, Ho, Er) [32–35].

Alike PVO films on LSAT substrates, the PVO films on LAO substrates show an abrupt increase in T_N with an increase in film thickness and approaches a nominal value for the thicker films [Fig. 4(d)]. Moreover, it is observed that the transition at T_{SO2} is present only for thicker films, and appears imperceptible for thinner films ($t < 55$ nm) [see inset of Fig. 4(c)]. Similarly, we observed a clear magnetic feature at T_{SO3} only for the thicker PVO/LAO films, and perhaps related to a different strain states between thinner and thicker films. Notably, the T_N of PVO films decreases with the decrease of film thickness, which is in contrast to the fact that "the compressive strain enhances the magnetic exchange interactions in PVO films, leading to an increase of T_N." This discrepancy probably results from the absence of T_{SO2} and T_{SO3} for the thinner PVO films, producing different magnetic ground states, and may be a change in the spin configuration, which are further arranged in a way as to decrease the exchange interaction between V-V neighboring sites, and thus lowering T_N of thinner PVO films.

Now we turn to the origin of this dead layer. For this, we investigate the valence states of the vanadium atomic species at different probing depths, by using x-ray photoelectron spectroscopy (XPS). Figure 5(a) shows the XPS spectra of a PVO film on the LSAT substrate at different probing depths of the film. We clearly observe a gradient of the V valence

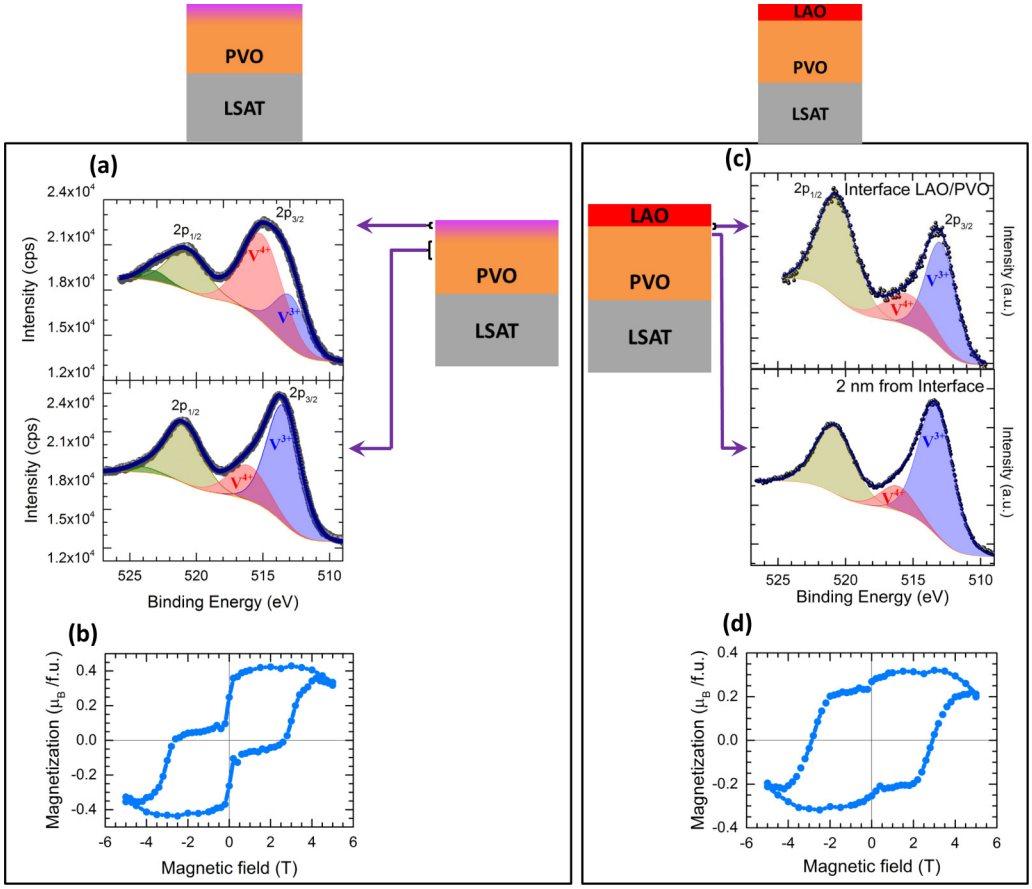

FIG. 5. (a) XPS spectra of V $2p$ core levels recorded on a 50-nm-thick PVO film grown on the LSAT substrate, near the film surface (upper panel) and at ∼10 nm probing depth (bottom panel). A clear gradient in the V valence state can be seen, leading to a higher concentration of V^{4+} at the film surface. The black spheres represent the original data, whereas color lines and shaded area are the fitted curves. (b) Corresponding magnetic hysteresis cycles obtained at 20 K for a 50-nm PVO/LSAT film. (c) XPS spectra of a LAO capped PVO film. The capping layer thickness is nearly 8 nm, and PVO film thickness is kept constant. The XPS spectra at different probing depths are shown; near LAO/PVO interface (upper panel) and 2 nm from the interface (bottom panel). Introduction of a capping layer clearly increases the formation of V^{3+} at the film surface (LAO/PVO interface). (d) Corresponding magnetic hysteresis cycles recorded at 20 K for the same capped LAO/PVO/LSAT film.

over the film depth, with a higher concentration of V^{4+} near the film surface. Also, as the probing depth increases, the V^{4+} concentration decreases [see Fig. 5(a)].

Then, to reduce the film surface, we use a capping layer of LAO (∼8 nm thick) grown *in situ* on top of PVO film by using PLD in the same deposition condition. The XPS results are shown in Fig. 5(c). One can see that the V^{3+} concentration at the surface of the film (interface of LAO/PVO) increases (compare to bare PVO film), whereas the formation of V^{4+} associated with the dead layer significantly decreases. With a further increase of the probing depth (from LAO/PVO interface) the V^{3+} concentration monotonically increases [bottom panel in Fig. 5(c)], and V^{4+} concentration decreases. Thus, these results indicate that the presence of V^{4+} at the surface of the film is likely at the origin of the dead layer. By comparing the magnetic hysteresis loops of the bare PVO [Fig. 5(b)] and the capped PVO [Fig. 5(d)], we confirm that the dead layer with a higher concentration of V^{4+} at the film surface is at the origin of the soft magnetic phase, which can be efficiently suppressed by the formation of more V^{3+} in the capped film. In addition, Fig. 5(d) clearly shows an improvement of the canted AFM properties of PVO capped with LAO, with a higher remanent magnetization, lower saturation magnetization, and larger H_c. More importantly, the soft magnetic component concomitant with the dead layer is strongly reduced.

In conclusion, we have investigated the effect of film thickness on the structural parameters (in-plane and out-of-plane) and magnetic properties of compressively strained $PrVO_3$ (PVO) thin films grown on $(La,Sr)(Al,Ta)O_3$ (LSAT) (100) (lattice misfit ∼0.8%) and $LaAlO_3$ (LAO) (100) (lattice misfit ∼2.9%) substrates, and evidenced a *dead layer* of $t \sim 4$–6 nm for both sample series. The less strained PVO/LSAT films ($\epsilon_{110} \sim 1.4\%$ for $t \sim 50$ nm) show highest $T_N \sim 120$ K, lower than bulk value, i.e., 130 K. On the other hand, the T_N of highly strained PVO/LAO films ($\epsilon_{110} \sim 2.5\%$ for $t \sim 50$ nm) raises up to ∼170 K, way above its counterpart bulk value. In addition, we have observed an increase in H_c and decrease in M_s with an increase in film thickness for both substrates, and

explained by the reduction in the proportion of paramagnetic phase. The XPS investigations of the films show that a higher concentration of V^{4+} at the surface of the film is responsible for this large paramagnetic M_s. A model based on the dead layer is used to quantify the thickness of the paramagnetic dead layer. Finally, we have attempted to cap the PVO film with ∼8 nm LAO film, in order to partially diminish the excess oxygen at the interface with PVO, and recover the magnetic properties related to the pure PVO. These observations suggest that the film thickness can be used to tune the strain/lattice deformation and thus functional properties in PVO thin films, and should be considered for other epitaxial perovskite thin films.

ACKNOWLEDGMENTS

The authors thank F. Veillon for his valuable experimental support. The authors also thank S. Froissart for the AFM support and L. Gouleuf for technical support. This work is supported by Region Normandie, by French ANR POLYNASH (ANR-17-CE08-0012) and Labex EMC3. M.S.R.R. and T.S.S. thank the Department of Science and Technology, New Delhi for funding which facilitated the establishment of the NFMTC (Grant No. SR NM/NAT/02-2005). M.S.R.R. received a fellowship for Invited Professor from University of Caen Normandie, and partial support from the LAFICS is also acknowledged. C.U.J. acknowledges University of Caen Normandie (UNICAEN) for visiting professorship.

[1] J. H. Haeni, P. Irvin, W. Chang, R. Uecker, P. Reiche, Y. L. Li, S. Choudhury, W. Tian, M. E. Hawley, B. Craigo, A. K. Tagantsev, X. Q. Pan, S. K. Streiffer, L. Q. Chen, S. W. Kirchoefer, J. Levy, and D. G. Schlom, Nature (London) **430**, 758 (2004).

[2] H. Meley, Karandeep, L. Oberson, J. de Bruijckere, D. T. L. Alexander, J.-M. Triscone, P. Ghosez, and S. Gariglio, APL Mater. **6**, 046102 (2018).

[3] S.-P. Matsuda, S. Takeuchi, A. Soeta, T. Doi, K. Aihara, and T. Kamo, Jpn. J. Appl. Phys. **29**, L1781 (1990).

[4] N. F. Mott, *Metal-Insulator Transitions* (Taylor and Francis, London, 1990).

[5] J.-S. Zhou, J. B. Goodenough, J.-Q. Yan, and Y. Ren, Phys. Rev. Lett. **99**, 156401 (2007).

[6] D. Bizen, K. Nakatsuka, T. Murata, H. Nakao, Y. Murakami, S. Miyasaka, and Y. Tokura, Phys. Rev. B **78**, 224104 (2008).

[7] A. T. Zayak, X. Huang, J. B. Neaton, and K. M. Rabe, Phys. Rev. B **74**, 094104 (2006).

[8] Z. Fan, J. Wang, M. B. Sullivan, A. Huan, D. J. Singh, and K. P. Ong, Sci. Rep. **4**, 4631 (2015).

[9] K. J. Choi, M. Biegalski, Y. L. Li, A. Sharan, J. Schubert, R. Uecker, P. Reiche, Y. B. Chen, X. Q. Pan, V. Gopalan, L.-Q. Chen, D. G. Schlom, and C. B. Eom, Science **306**, 1005 (2004).

[10] D. Kumar, A. David, A. Fouchet, A. Pautrat, J. Varignon, C. U. Jung, U. Lüders, B. Domengès, O. Copie, P. Ghosez, and W. Prellier, Phys. Rev. B **99**, 224405 (2019).

[11] M. H. Sage, G. R. Blake, C. Marquina, and T. T. M. Palstra, Phys. Rev. B **76**, 195102 (2007).

[12] S. Miyasaka, Y. Okimoto, M. Iwama, and Y. Tokura, Phys. Rev. B **68**, 100406(R) (2003).

[13] O. Copie, J. Varignon, H. Rotella, G. Steciuk, P. Boullay, A. Pautrat, A. David, B. Mercey, P. Ghosez, and W. Prellier, Adv. Mater. **29**, 1604112 (2017).

[14] K. I. Kugel and D. I. Khomskii, Zh. Eksp. Teor. Fiz. **64**, 1429 (1973).

[15] O. Copie, H. Rotella, P. Boullay, M. Morales, A. Pautrat, P.-E. Janolin, I. C. Infante, D. Pravathana, U. Lüders, and W. Prellier, J. Phys.: Condens. Matter **25**, 492201 (2013).

[16] C.-J. Cheng, C. Lu, Z. Chen, L. You, L. Chen, J. Wang, and T. Wu, Appl. Phys. Lett. **98**, 242502 (2011).

[17] S. Valencia, L. Balcells, B. Martínez, and J. Fontcuberta, J. Appl. Phys. **93**, 8059 (2003).

[18] P. Kaur, K. K. Sharma, R. Pandit, R. J. Choudhary, and R. Kumar, Appl. Phys. Lett. **104**, 081608 (2014).

[19] K. Yoshimatsu, T. Okabe, H. Kumigashira, S. Okamoto, S. Aizaki, A. Fujimori, and M. Oshima, Phys. Rev. Lett. **104**, 147601 (2010).

[20] T. M. Dao, P. S. Mondal, Y. Takamura, E. Arenholz, and J. Lee, Appl. Phys. Lett. **99**, 112111 (2011).

[21] A. Biswas and Y. H. Jeong, J. Appl. Phys. **117**, 195305 (2015).

[22] U. Aschauer, R. Pfenninger, S. M. Selbach, T. Grande, and N. A. Spaldin, Phys. Rev. B **88**, 054111 (2013).

[23] J. Scola, P. Boullay, W. Noun, E. Popova, Y. Dumont, A. Fouchet, and N. Keller, J. Appl. Phys. **110**, 043928 (2011).

[24] J. Scola, W. Noun, E. Popova, A. Fouchet, Y. Dumont, N. Keller, P. Lejay, I. Sheikin, A. Demuer, and A. Pautrat, Phys. Rev. B **81**, 174409 (2010).

[25] See Supplemental Material at http://link.aps.org/supplemental/10.1103/PhysRevMaterials.3.124413 for details of the evolution of M_s and H_c (extracted from hysteresis loops at $T = 30$ K) with film thickness, and fit of the proposed model to the observed M_s vs t (at $T = 20$ and 30 K) to estimate the thickness of the dead layer.

[26] R. Aeschlimann, D. Preziosi, P. Scheiderer, M. Sing, S. Valencia, J. Santamaria, C. Luo, H. Ryll, F. Radu, R. Claessen, C. Piamonteze, and M. Bibes, Adv. Mater. **30**, 1707489 (2018).

[27] Y. Hotta, H. Wadati, A. Fujimori, T. Susaki, and H. Y. Hwang, Appl. Phys. Lett. **89**, 251916 (2006).

[28] A. Fouchet, J. E. Rault, M. Allain, B. Bérini, J.-P. Rueff, Y. Dumont, and N. Keller, J. Appl. Phys. **123**, 055302 (2018).

[29] F. Wang, J. Zhang, P. Yuan, Q. Yan, and P. Zhang, J. Phys.: Condens. Matter **12**, 3037 (2000).

[30] X. Zhou, Z. Wang, S. Ge, D. Wang, J. Yu, and D. Yao, Phys. Status Solidi A **211**, 2839 (2014).

[31] F. Zhang, S. Ge, Z. Wang, X. Zhou, G. Wang, Z. Yu, and F. Li, J. Alloys Compd. **506**, 109 (2010).

[32] M. Reehuis, C. Ulrich, K. Prokeš, S. Mat'aš, J. Fujioka, S. Miyasaka, Y. Tokura, and B. Keimer, Phys. Rev. B **83**, 064404 (2011).

[33] M. Reehuis, C. Ulrich, P. Pattison, B. Ouladdiaf, M. C. Rheinstädter, M. Ohl, L. P. Regnault, M. Miyasaka, Y. Tokura, and B. Keimer, Phys. Rev. B **73**, 094440 (2006).

[34] M. Reehuis, C. Ulrich, P. Pattison, M. Miyasaka, Y. Tokura, and B. Keimer, Eur. Phys. J. B **64**, 27 (2008).

[35] M. Reehuis, C. Ulrich, P. M. Abdala, P. Pattison, G. Khaliullin, J. Fujioka, S. Miyasaka, Y. Tokura, and B. Keimer, Phys. Rev. B **94**, 104436 (2016).